Catalysis Science & Technology

Accepted Manuscript

ROYAL SOCIETY OF CHEMISTRY

www.rsc.org/catalysis

Journal Name

RSCPublishing

ARTICLE

(Pd-$CuCl_2$)/γ-Al_2O_3: a high-performance catalyst for carbonylation of methyl nitrite to dimethyl carbonate†

Cite this: DOI: 10.1039/x0xx00000x

Received 00th January 2012,
Accepted 00th January 2012

DOI: 10.1039/x0xx00000x

www.rsc.org/

Dong-Mei Lv,[a,b] Zhong-Ning Xu,*[a] Si-Yan Peng,[a] Zhi-Qiao Wang,[a] Qing-Song Chen,[a] Yumin Chen,[a] Guo-Cong Guo*[a]

(Pd-$CuCl_2$)/γ-Al_2O_3 catalyst with excellent activity and selectivity has been successfully developed for vapor-phase carbonylation of methyl nitrite to dimethyl carbonate (DMC). It has been demonstrated that the Cl^- is necessary for the superior selectivity (99.8%) to DMC, and Cl^- and Cu^{2+} have synergetic effect. The Lewis acid sites of support γ-Al_2O_3 may be suitable for vapor-phase carbonylation of methyl nitrite to DMC. Moreover, the catalytic mechanism of DMC formation on (Pd-$CuCl_2$)/γ-Al_2O_3 catalyst has been reasonably proposed based on the results of XPS and *in situ* diffuse reflectance infrared spectroscopy. The intermediate Cl-Pd(II)-$COOCH_3$ is the key factor for the synthesis of DMC.

1. Introduction

Dimethyl carbonate (DMC) is a low-toxic and environmentally friendly industrial chemical, which has been widely applied in many organic reactions, owing to its methyl groups and carbonyl group.[1] It can be used as an attractive alternative to phosgene and methyl halides (or dimethyl sulfate) for carbonylation and methylation processes, respectively.[2, 3] DMC is also a potential fuel additive due to its high oxygen content, low toxicity and rapid biodegradability.[4] In addition, it has been mentioned as electrolyte in lithium batteries because of its excellent dissolving performance and low viscosity.[5]

Considerable efforts have been dedicated to study the synthesis of DMC due to its great application. Until now, several synthetic methods of DMC have been developed, such as phosgenation,[6] transesterification route,[7] liquid-phase methanol oxycarbonylation,[8, 9] vapor-phase methanol oxycarbonylation,[3, 10-12] and vapor-phase carbonylation of methyl nitrite (MN).[13, 14] Among these synthetic routes, vapor-phase carbonylation of MN has drawn much attention, because it has many great advantages compared with the other methods. There is no byproduct water in the process of the DMC synthesis by this route, which can avoid the problem of separation and enhance the stability of catalyst. Moreover, the reaction condition of this route is mild, which can be realized under an atmospheric pressure and low temperature at 90–130 °C.[15]

Pd-based and Cu-based catalysts both have been widely applied in various industrial processes, such as CO oxidative coupling to dimethyl oxalate[16-18] and chemoselective hydrogenation of dimethyl oxalate to ethylene glycol.[19] Moreover, several supported palladium or copper catalysts have also been used in the formation of DMC by vapor-phase carbonylation of MN, such as Pd/NaY,[13] Pd/FAU,[14] $PdCl_2$-$CuCl_2$/$LiAl_5O_8$,[20] and $PdCl_2$/activated carbon (AC),[21] with the selectivity to DMC being 85%, 85%, 92% and 96%, respectively. Although the catalytic activities of these catalysts have been enhanced, the catalytic activities are still not very high (354 to 1200 $g \cdot L^{-1} \cdot h^{-1}$), and can be further upgraded. Most importantly, the influencing factors of catalytic activities are uncertain up to now. In addition, several supports have been reported for the formation of DMC, such as zeolite, AC, silica and alumina.[15, 21] And the catalytic performance of catalysts are different with different supports, suggesting that the nature properties of the catalyst carriers are important factors influencing the catalytic performance. However, the details of supports influencing the catalytic performance are not really clear, which still need further efforts to afford on it.

In this work, we developed a high-performance (Pd-$CuCl_2$)/γ-Al_2O_3 catalyst for vapor-phase carbonylation of MN to DMC. The influencing factors of catalytic activities have been investigated in details. We also reasonably proposed the catalytic mechanism on (Pd-$CuCl_2$)/γ-Al_2O_3 catalyst based on the results of XPS and *in situ* diffuse reflectance infrared spectroscopy.

2. Experimental section

2.1 Materials

Palladium acetate (AR; Sino-Platinum Co., Ltd, China); $CuCl_2 \cdot 2H_2O$, $CuSO_4 \cdot 5H_2O$, KCl, γ-Al_2O_3, α-Al_2O_3, and MgO

(AR; Aladdin Reagent Co., Ltd, China); acetone (AR; Sinopharm Chemical Reagent Co., Ltd, China); the mixed gas of CO/N_2/Ar (35%/60%/5%; purchased from Xinhang Industrial Gases Co., Ltd, China); MN (99%; prepared by the reaction of methanol, sodium nitrite and concentrated sulfuric acid in a device invented by ourselves (CN102372637B, CN202359045U).

2.2 Catalyst preparation

Pd/γ-Al_2O_3 catalyst with 0.5 wt% theoretical Pd loading was prepared by wet-impregnation method. The process is described as follows. Firstly, adding γ-Al_2O_3 into an acetone solution of palladium acetate under vigorous stirring, and then stirring the mixture slurry for 12 h. The resulting solid was dried at 40 °C in a vacuum drying oven, calcined at 400 °C in static air for 2 h and then reduced under pure H_2 atmosphere at 400 °C for 2 h to obtain Pd/γ-Al_2O_3 catalyst. (Pd-$CuCl_2$)/γ-Al_2O_3 catalyst was prepared by mixing 0.1 g Pd/γ-Al_2O_3 catalyst with 0.1 g milled $CuCl_2 \cdot 2H_2O$ crystal in designated Pd/Cu molar ratios (as shown in Table 1).

The preparation processes of (Pd-$CuSO_4$)/γ-Al_2O_3, (Pd-KCl)/γ-Al_2O_3 and (Pd-$CuSO_4$-KCl)/γ-Al_2O_3 catalysts were the same as the preparation process of (Pd-$CuCl_2$)/γ-Al_2O_3 catalyst, except the mixed agents are $CuSO_4$, KCl, and $CuSO_4$-KCl, respectively.

(Pd-$CuCl_2$)/α-Al_2O_3 and (Pd-$CuCl_2$)/MgO catalysts were prepared by the same process of (Pd-$CuCl_2$)/γ-Al_2O_3 catalyst, except the support γ-Al_2O_3 was changed to α-Al_2O_3 and MgO, respectively.

2.3 Catalyst characterization

X-ray photoelectron spectroscopy (XPS) analysis was performed with a VG Escalab 250 spectrometer equipped with an X-ray source by employing Al-Kα (1486.7 eV) anode.

Inductively coupled plasma (ICP) spectroscopy was recorded with an Ultima 2 plasma emission spectrometer from Jobin Yvon.

X-ray diffraction (XRD) patterns were recorded on a glass wafer by a Rigaku MiniFlex II diffractometer with a slit of 1.25 ° at a scanning rate of 10 °/min using Cu-Kα radiation (λ = 1.5406 Å).

Samples for transmission electron microscopy (TEM), scanning transmission electron microscopy (STEM) and high resolution TEM (HRTEM) observations were prepared by drying a drop of diluted ethanol dispersion of (Pd-$CuCl_2$)/γ-Al_2O_3 catalysts on copper grids. Particle sizes and shapes were examined by a TEM (JEM-2010) operated at 200 kV.

The acid properties of the supports were detected by NH_3 temperature programmed desorption (NH_3-TPD) technique. The detail experimental process is as follows. 100 mg of sample was treated with Helium at 400 °C for 1 h to remove the adsorbed impurities. After cooling to 25 °C under a He flow, the sample was exposed to 20% NH_3-He mixture (50 mL·min^{-1}) for 1 h, followed by purging with He for 30 min, and then heated to 400 °C by ramping at 10 °C·min^{-1} under flowing He.

The BET surface area of samples was determined by N_2 adsorption-desorption at liquid nitrogen temperature (77 K), which was performed on Micromeritics ASAP 2020. The surface areas were calculated from the isotherms using the Brunauere Emmette Teller (BET) method. The total pore volume was calculated from the amount of N_2 adsorbed when $P/P_0 = 0.95$.

Fourier transform infrared spectroscopy of NH_3 (NH_3-FTIR) spectra were recorded on a Nicolet 6700 diffuse reflectance infrared spectrometer equipped with a stainless steel *in situ* IR flow cell. The powder samples were placed into the cell and had been pretreated under flowing N_2 for 30 min at 300 °C. After cooling down to 110 °C, a reference spectrum was recorded. Then, the NH_3 was introduced in constant flowing for 30 min and the spectra were recorded in the range of 4000–650 cm^{-1} at a resolution of 4 cm^{-1}. Subsequently, the samples were swept by N_2 flow for a while and the spectra were recorded in the range of 4000–650 cm^{-1} again.

In situ diffuse reflectance infrared spectroscopy (DRIRS) measurements were performed on a Nicolet 6700 diffuse reflectance infrared spectrometer equipped with a stainless steel *in situ* IR flow cell. The powder samples were placed into the cell and had been pretreated under flowing N_2 for 30 min at 150 °C. After cooling down to the 120 °C, a reference spectrum was recorded. Then, the reactants were introduced in constant flowing and the spectra were recorded at a resolution of 4 cm^{-1}.

2.4 Catalytic activity evaluation

Catalytic activities of as-synthesized catalysts for vapor-phase carbonylation of MN to DMC were measured by a fixed-bed quartz tubular reactor. The center of quartz tubular reactor was loaded with 200 mg of catalysts. This reaction was performed under atmospheric pressure using reactant gases composing of 23.4% CO, 33% MN, 3.4% Ar (as internal standard), and 40.2% N_2 (as balance gas) at a gas hourly space velocity (GHSV) of 3000 h^{-1} and temperance of 120 °C. The composition of the reactant gases and reaction products was monitored using an on-line Shimadzu GC-2014 gas chromatograph equipped with a thermal conductivity detector and a flame ionization detector.

The conversion of CO, the selectivity to DMC and the space-time yields (STY) of DMC were calculated using the following formulas:

Conversion of CO (%) = $([CO]_{in}/[Ar]_{in} - [CO]_{out}/[Ar]_{out})/([CO]_{in}/[Ar]_{in}) \times 100\%$

Due to the molar ratio of CO and CH_3ONO is 0.7 : 1, the maximal conversion of CO is 71.4%.

Selectivity to DMC (%) = $(S_{DMC} \times R\text{-}F_{DMC})/(S_{DMC} \times R\text{-}F_{DMC} + S_{DMO} \times R\text{-}F_{DMO}) \times 100\%$

STY of DMC ($g \cdot L^{-1} \cdot h^{-1}$) = conversion of CO × selectivity to DMC × GHSV of CO h^{-1} × 90.08 $g \cdot mol^{-1}/(22.4\ L \cdot mol^{-1})$

where $[Ar]_{in}$ and $[Ar]_{out}$ are the concentrations of Ar at the inlet

Table 1. Catalytic activities of as-synthesized catalysts[a].

Catalysts	Actual Pd loading (%)	Actual Cu loading (%)	Actual K loading (%)	Conversion of CO (%)	Selectivity[b] to DMC (%)	STY[c] of DMC ($g \cdot L^{-1} \cdot h^{-1}$)
$Pd/\gamma\text{-}Al_2O_3$	0.44	-	-	46.0	23.5	299
$(Pd\text{-}KCl)/\gamma\text{-}Al_2O_3$	0.20	-	26.47	30.1	93.8	784
$(Pd\text{-}CuSO_4)/\gamma\text{-}Al_2O_3$	0.21	15.76	-	35.0	21.4	207
$(Pd\text{-}CuSO_4\text{-}KCl)/\gamma\text{-}Al_2O_3$	0.21	7.88	10.51	39.4	99.7	1090
$(Pd\text{-}CuCl_2)/\gamma\text{-}Al_2O_3$	0.24	18.18	-	70.9	99.8	1963
$CuCl_2/\gamma\text{-}Al_2O_3$	-	18.26	-	8.4	99.1	231

[a] Reaction conditions: 200 mg of catalyst, 3000 h^{-1} of gas hourly space velocity (GHSV), reactants CO/MN/Ar/N_2 volume ratio: 23.4 : 33 : 3.4 : 40.2, 0.1 MPa, 120 °C.

[b] Selectivity to DMC based on CO. [c] STY represents the space-time yield, grams of DMC per liter of catalyst per hour ($g \cdot L^{-1} \cdot h^{-1}$).

and outlet, $[CO]_{in}$ and $[CO]_{out}$ are the concentration of CO at the inlet and outlet, respectively. S_{DMC} and S_{DMO} are the peak areas of dimethyl carbonate and dimethyl oxalate and $R\text{-}F_{DMC}$ and $R\text{-}F_{DMO}$ are the relative correction factors of dimethyl carbonate and dimethyl oxalate, respectively.

3. Results and discussion

3.1 Catalytic activity and the influencing factors

The actual Pd, Cu, K loadings and catalytic activities of as-synthesized catalysts are shown in Table 1. The actual Pd loading of $Pd/\gamma\text{-}Al_2O_3$ catalyst is 0.44%. The selectivity to DMC over $Pd/\gamma\text{-}Al_2O_3$ catalyst is only 23.5%. When KCl was introduced into the $Pd/\gamma\text{-}Al_2O_3$ catalyst, the selectivity to DMC over $(Pd\text{-}KCl)/\gamma\text{-}Al_2O_3$ catalyst was drastically increased to 93.8%, implying that the Cl^- is important for the selectivity to DMC. When KCl was changed to $CuSO_4$, the conversion of CO and selectivity to DMC over $(Pd\text{-}CuSO_4)/\gamma\text{-}Al_2O_3$ catalyst were both decreased slightly. However, when KCl and $CuSO_4$ were both introduced, the conversion of CO and selectivity to DMC over $(Pd\text{-}CuSO_4\text{-}KCl)/\gamma\text{-}Al_2O_3$ catalyst were higher than those over $(Pd\text{-}KCl)/\gamma\text{-}Al_2O_3$ catalyst, suggesting that Cl^- and Cu^{2+} may have synergistic effect. Thus, when $CuCl_2$ was introduced, the conversion of CO over $(Pd\text{-}CuCl_2)/\gamma\text{-}Al_2O_3$ catalyst reached up to 70.9%, which is close to the maximal conversion of CO (71.4%), and the selectivity to DMC over $(Pd\text{-}CuCl_2)/\gamma\text{-}Al_2O_3$ catalyst also reached up to 99.8%, implying that the Cl^- is necessary for the superior selectivity to DMC,[15] the Cu^{2+} only in the $CuCl_2$ form can greatly promote the catalytic activity, and the Cl^- and Cu^{2+} have synergistic effect indeed. In additon, the conversion of CO and the selectivity to DMC over $CuCl_2/\gamma\text{-}Al_2O_3$ catalyst are 8.4% and 99.1%, respectively, suggesting that $CuCl_2$ is a co-catalyst for vapor-phase carbonylation of MN to DMC.

TEM image of $(Pd\text{-}CuCl_2)/\gamma\text{-}Al_2O_3$ catalyst is shown in Fig. 1a, which cannot clearly presented Pd nanoparticles dispersed on the $\gamma\text{-}Al_2O_3$ support. Thus, STEM image was employed (Fig. 1c), which is obvious to find that Pd nanoparticles of $(Pd\text{-}CuCl_2)/\gamma\text{-}Al_2O_3$ catalyst are highly dispersed on the $\gamma\text{-}Al_2O_3$ support. And the HRTEM image (Fig. 1b) reveals that the interval between two lattice fringes of Pd nanoparticles is *ca.* 0.226 nm, which corresponds to the interplanar distance of the (111) plane of the face-centered cubic (fcc) Pd.[17] Size distribution histograms presented in Fig. 1d demonstrate the average size of Pd nanoparticles of $(Pd\text{-}CuCl_2)/\gamma\text{-}Al_2O_3$ catalyst is 3.86 nm, indicating that the Pd nanoparticles are small and uniform.

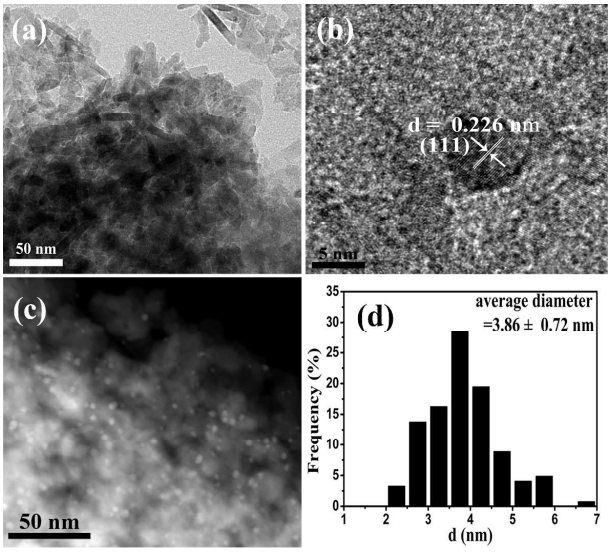

Fig. 1. (a) TEM, (b) HRTEM, (c) STEM images and (d) size distributions of Pd nanoparticles of $(Pd\text{-}CuCl_2)/\gamma\text{-}Al_2O_3$ catalyst.

Table 2. Catalytic activities of as-synthesized catalysts with different supports.

Catalysts	Actual Pd loading (%)	Actual Cu loading (%)	Conversion of CO (%)	Selectivity to DMC (%)	STY of DMC ($g \cdot L^{-1} \cdot h^{-1}$)
(Pd-$CuCl_2$)/γ-Al_2O_3	0.24	18.18	70.9	99.8	1963
(Pd-$CuCl_2$)/α-Al_2O_3	0.20	17.16	12.7	53.2	187
(Pd-$CuCl_2$)/MgO	0.27	18.64	6.3	92.5	161

In addition, the XRD patterns of $CuCl_2$ and (Pd-$CuCl_2$)/γ-Al_2O_3 are shown in Fig. S1. Compared with the diffraction peaks of pure $CuCl_2$ (Fig. S1a), the sharp diffraction peaks of (Pd-$CuCl_2$)/γ-Al_2O_3 can be assigned to the crystalline phase of the $CuCl_2$ (Fig. S1b). Besides, no Pd diffraction peaks were observed for (Pd-$CuCl_2$)/γ-Al_2O_3 catalyst, indicating that Pd nanoparticles are highly dispersed on the surface of γ-Al_2O_3, which is consistent with the result of STEM characterization.

3.2 Effect of Lewis acid sites of supports on catalytic activities

In order to investigate the effect of Lewis acid and base sites of supports on catalytic activities, (Pd-$CuCl_2$)/γ-Al_2O_3, (Pd-$CuCl_2$)/α-Al_2O_3 and (Pd-$CuCl_2$)/MgO catalysts have been synthesized and evaluated under the same reaction conditions. The actual Pd, Cu loadings and catalytic activities of as-synthesized catalysts are shown in Table 2. The order of catalytic activity is (Pd-$CuCl_2$)/γ-Al_2O_3 >> (Pd-$CuCl_2$)/α-Al_2O_3 > (Pd-$CuCl_2$)/MgO, suggesting that the acid and base sites of supports would strongly affect the catalytic activity, and the γ-Al_2O_3 is a much better suitable support for vapor-phase carbonylation of MN to DMC.

In addition, the nitrogen adsorption-desorption isotherms of (Pd-$CuCl_2$)/γ-Al_2O_3, (Pd-$CuCl_2$)/α-Al_2O_3, (Pd-$CuCl_2$)/MgO and Pd/γ-Al_2O_3 catalysts are shown in Fig. S2 and the texture properties of as-synthesized catalysts with different supports are shown in Table S1. It is obvious to find that both the BET surface area and pore volume of (Pd-$CuCl_2$)/γ-Al_2O_3 catalyst are much higher than (Pd-$CuCl_2$)/α-Al_2O_3 and (Pd-$CuCl_2$)/MgO catalysts, implying that large BET surface area and pore volume of support might be benefit for vapor-phase carbonylation of MN to DMC.

NH_3-TPD profiles (Fig. 2) have been performed to analyze the acid characteristics of Pd-$CuCl_2$ catalysts with different supports. There are several NH_3 desorption peaks in Fig. 2, which can be classified into three types of acid sites with different intensity, *i.e.*, "weak" (NH_3 desorption between 50 and 210 °C), "medium" (NH_3 desorption between 210 and 400 °C) and "strong" (NH_3 desorption between above 400 °C). The "weak" acid are might assigned to NH_3 absorbed by physics and NH_3 adsorbed on weak Lewis acid sites. And the "medium" and "strong" acid are probably associated with NH_3 absorbed on strong Lewis acid sites and Brønsted acid sites.[22, 23] Too much Brønsted acid is harmful to the reaction of vapor-phase carbonylation of MN to DMC, which is in accord with that the abundant Brønsted acidic sites of supports may be in favor of the formation of by-products methanol, methyl formate and dimethoxymethane by enhancing the decomposition of MN.[14, 24-26] As shown in Fig. 2, it is obvious to find that the amount of both "weak" and "medium" acid sites of (Pd-$CuCl_2$)/γ-Al_2O_3 is larger than those of other catalysts with α-Al_2O_3 or MgO as support, suggesting that γ-Al_2O_3 are beneficial to vapor-phase carbonylation of MN to DMC.

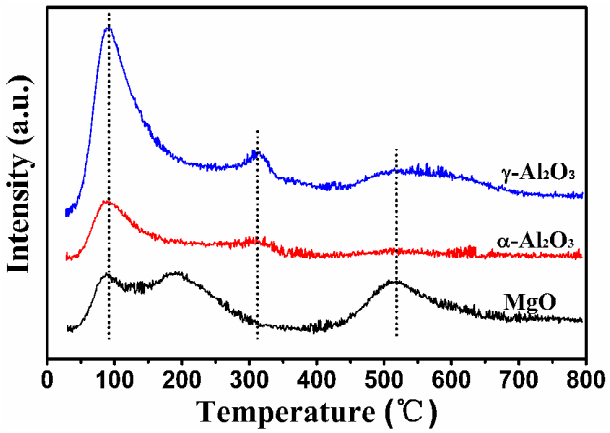

Fig. 2. NH_3-TPD profiles of Pd-$CuCl_2$ catalysts with different supports.

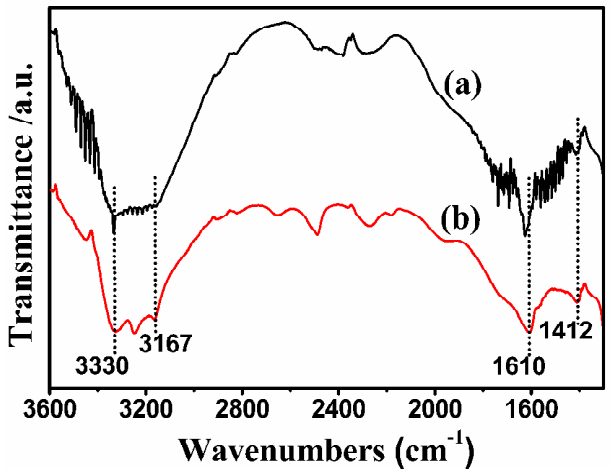

Fig. 3. NH_3-FTIR spectra of (Pd-$CuCl_2$)/γ-Al_2O_3 catalyst: (a) exposure to NH_3, (b) swept by N_2.

NH_3-FTIR (Fig. 3) of (Pd-$CuCl_2$)/γ-Al_2O_3 catalyst was further carried out to distinguish the Lewis acid sites and Brønsted acid sites. After sweeping by N_2, the typical peaks (Fig. 3b) are obvious. The peaks at about 3330 and 1610 cm^{-1} are ascribed to NH_3 adsorbed on the center of Lewis acid sites, while the peaks at about 3167 and 1412 cm^{-1} are assigned to NH_3 adsorbed on the center of Brønsted acid sites. The peak areas of Lewis acid sites are relatively larger than those of Brønsted acid sites, which indicates that the Lewis acid sites of γ-Al_2O_3 may be conducive to produce DMC in the present of Cl^- at the same time.[14]

3.3 Catalytic mechanism on (Pd-$CuCl_2$)/γ-Al_2O_3 catalyst

Pd 3d XPS spectra of the fresh and engaged (Pd-$CuCl_2$)/γ-Al_2O_3 catalysts are shown in Fig. 4. The binding energies (BE) of Pd $3d_{5/2}$ and $3d_{3/2}$ peaks for the fresh (Pd-$CuCl_2$)/γ-Al_2O_3 catalyst (Fig. 4a) are at 335.17 and 340.16 eV, respectively, indicating that the state of Pd in the fresh (Pd-$CuCl_2$)/γ-Al_2O_3 catalyst is Pd(0).[13, 14, 16, 27] While the BE of Pd $3d_{5/2}$ and $3d_{3/2}$ for the engaged (Pd-$CuCl_2$)/γ-Al_2O_3 catalyst (Fig. 4b) are at 337.93 eV and 342.82 eV, respectively, which are ascribed to Pd(II).[13, 14, 16, 27] It can be proposed that Pd(0) in the fresh (Pd-$CuCl_2$)/γ-Al_2O_3 catalyst was oxidized to Pd(II) by MN and $CuCl_2$, and the intermediate Cl-Pd(II)-OCH_3 might be formed.[15]

Cu 2p XPS spectra of the fresh and engaged (Pd-$CuCl_2$)/γ-Al_2O_3 catalysts are shown in Fig. S3. The BE of Cu $2p_{3/2}$ and Cu $2p_{1/2}$ peaks for the fresh (Pd-$CuCl_2$)/γ-Al_2O_3 catalyst (Fig. S3a) are at 934.2 and 954.1 eV, respectively, indicating that the oxidation state of Cu in the fresh (Pd-$CuCl_2$)/γ-Al_2O_3 catalyst is Cu(II)[28, 29]. The BE of Cu $2p_{3/2}$ and Cu $2p_{1/2}$ peaks for the engaged (Pd-$CuCl_2$)/γ-Al_2O_3 catalyst (Fig. S3b) are at 934.5 eV and 954.2 eV, respectively, which are also ascribed to Cu(II)[28, 29]. Under the oxidizing atmosphere of MN, the Cu(I)Cl might be quickly oxidized to Cl-Cu(II)-OCH_3. Thus, the Cu(I) was not detected by XPS.

The *in situ* DRIRS of CO adsorption on (Pd-$CuCl_2$)/γ-Al_2O_3 catalyst is shown in Fig. S4. The peaks at 2162 and 2127 cm^{-1} are attributed to the bimodal of CO in gas,[30, 31] while the peaks at 1998 and 1932 cm^{-1} are assigned to adsorbed CO on surface of Pd in bridge (Pd_2–CO).[32, 33] The *in situ* DRIRS of MN adsorption on (Pd-$CuCl_2$)/γ-Al_2O_3 catalyst has been measured at 120 °C (Fig. 5). As presented in Fig. 5a, the peaks at 2962 and 2844 cm^{-1} are attributed to anti-symmetric and symmetric C–H stretching vibrations of the CH_3– in MN, while the peaks at 1445 and 1378 cm^{-1} (Fig. 5b) can be assigned to CH_3– deformation vibrations of MN.[34] The peaks at 1686 and 1668 cm^{-1}, 1635 and 1612 cm^{-1} can be ascribed to symmetric and anti-symmetric N=O stretching vibrations of MN, respectively,[16] as shown in Fig. 5b. Meanwhile, the peaks at 3336 and 3317 cm^{-1}, 3227 and 3210 cm^{-1} are ascribed to anti-symmetric and symmetric overtone of N=O stretching vibrations of MN, respectively,[35] as shown in Fig. 5a. Besides,

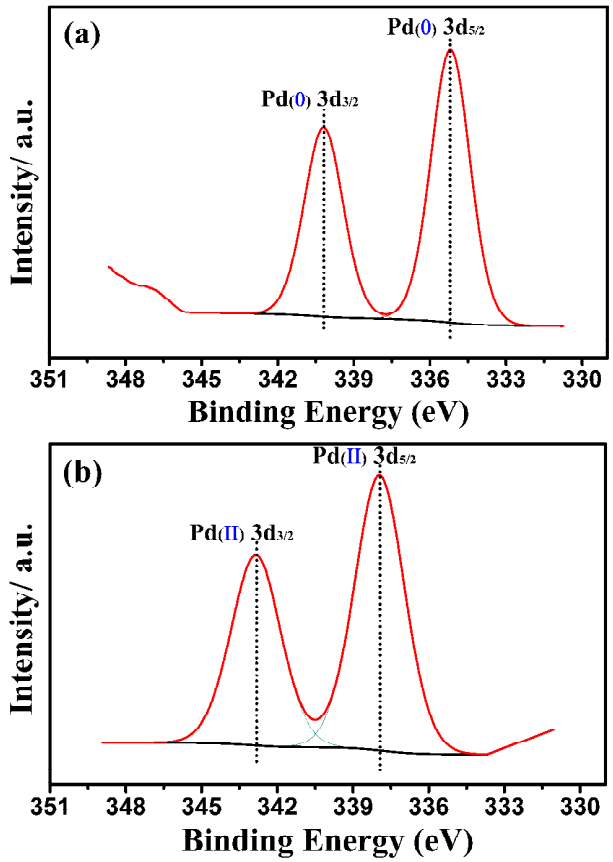

Fig. 4. Pd 3d XPS spectra of (a) fresh and (b) engaged (Pd-$CuCl_2$)/γ-Al_2O_3 catalysts.

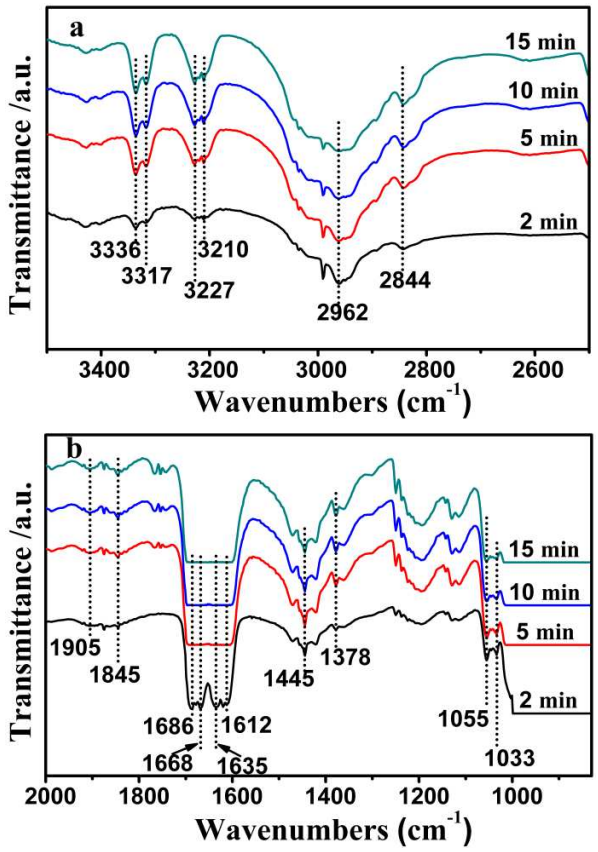

Fig. 5. *In situ* DRIR spectra of MN on (Pd-$CuCl_2$)/γ-Al_2O_3 catalyst at 120 °C: (a) range from 3500 to 2500 cm^{-1}; (b) range from 2000 to 1000 cm^{-1}.

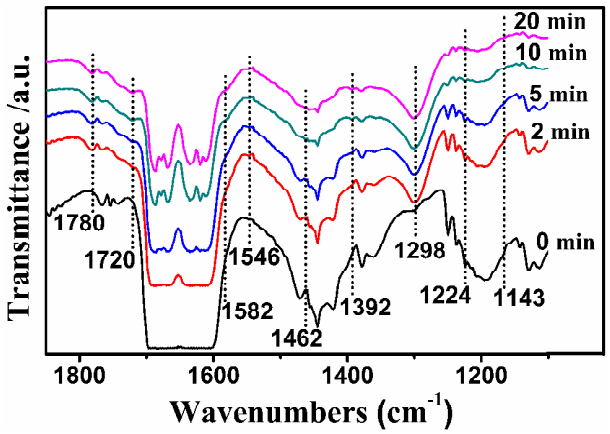

Fig. 6. *In situ* DRIR spectra of the reaction between CO and MN on (Pd-$CuCl_2$)/γ-Al_2O_3 catalyst at 120 °C, range from 1850 to 1100 cm^{-1}.

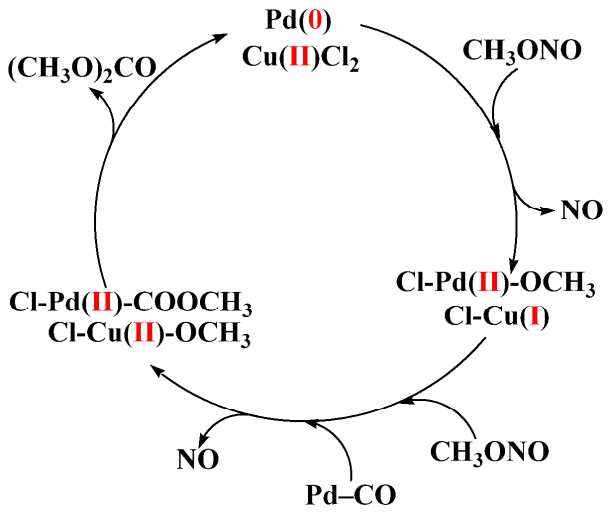

Fig. 7. The proposed catalytic mechanism of DMC formation on (Pd-$CuCl_2$)/γ-Al_2O_3 catalyst.

from Fig. 5b, evidence for adsorbed CH_3O– species on the surface of (Pd-$CuCl_2$)/γ-Al_2O_3 catalyst is given by the peaks observed at 1055 and 1033 cm^{-1}, which are attributed to C–O stretching vibrations,[34] while the bands appeared at 1845 and 1905 cm^{-1}, 1742 and 1756 cm^{-1} are assigned to the bimodal of gaseous NO and gaseous methyl formate, respectively, which should be due to the part dissociation of MN.[35, 36] It is worthy to note that the intensities of the peaks at 1845 and 1905 cm^{-1} were increased with the passing of time, implying that the adsorbed CH_3O– species on the surface of (Pd-$CuCl_2$)/γ-Al_2O_3 catalyst are associated with the formation of the intermediate Cl–Pd(II)–OCH_3.

In situ DRIRS of the reaction between CO and MN on (Pd-$CuCl_2$)/γ-Al_2O_3 catalyst has further been measured at 120 °C (Fig. 6). The peak at 1720 cm^{-1} is ascribed to C=O stretching vibrations of monomethyl carbonate (MMC, namely CH_3OOC–) species associated with Pd in (Pd-$CuCl_2$)/γ-Al_2O_3 catalyst, which is associated with the formation of the another intermediate Cl–Pd(II)–$COOCH_3$. It is worth noting that a couple of new peaks appeared at 1392 cm^{-1} and 1546 cm^{-1} are attributed to anti-symmetric stretching and symmetric stretching of O–C–O in MMC species, which have been increased with the passing of time. Moreover, the bands ranging from 1143 to 1224 cm^{-1} could be due to C–O–C vibration of the intermediate Cl–Pd(II)–$COOCH_3$.[34, 35] On the other hand, the peaks at 2869 cm^{-1} (as shown in Fig. S5) and 1462 cm^{-1} are assigned to symmetric stretching[34, 37-39] and deforming C–H vibrations[34] of the CH_3– in DMC, respectively. Importantly, a couple of new strong peaks at 1780 cm^{-1} and 1298 cm^{-1} appeared with the passing of time, which are assigned to C=O stretching and C–O stretching in gaseous DMC, respectively.[34]

The catalytic mechanism of DMC formation on (Pd-$CuCl_2$)/γ-Al_2O_3 catalyst was reasonably proposed as shown in Fig. 7. Firstly, Pd(0) was oxidized to Pd(II) by MN and $CuCl_2$, and formed the intermediates Cl-Pd(II)-OCH_3 and Cu(I)Cl, which was supported by XPS and *in situ* DRIRS of MN. Secondly, the insertion reaction between the intermediate Cl-Pd(II)-OCH_3 and CO absorbed on Pd was carried out to form another intermediate Cl-Pd(II)-$COOCH_3$, which was supported by *in situ* DRIRS of the reaction between CO and MN. Meanwhile, Cu(I)Cl was oxidized by another MN to form Cl-Cu(II)-OCH_3. Finally, the intermolecular elimination reaction happened between the intermediates Cl-Pd(II)-$COOCH_3$ and Cl-Cu(II)-OCH_3, which caused the formation of DMC, the recovery of $CuCl_2$ and the reduction of Pd(II) to Pd(0).

Conclusion

In summary, we have successfully developed a high-performance (Pd-$CuCl_2$)/γ-Al_2O_3 catalyst for vapor-phase carbonylation of MN to DMC, and further discovered that the Cl^- is quite important for the excellent selectivity to DMC, and Cl^- and Cu^{2+} have synergetic effect. γ-Al_2O_3 was demonstrated to be an excellent support for Pd-$CuCl_2$ catalyst due to its abundant Lewis acid sites. The catalytic mechanism of DMC formation on (Pd-$CuCl_2$)/γ-Al_2O_3 catalyst has been reasonably proposed based on the characterization results of XPS and *in situ* DRIRS. The intermediate Cl-Pd(II)-$COOCH_3$ is the key factor for the synthesis of DMC. This work could provide insights for developing practical industrial catalyst for vapor-phase carbonylation of MN to DMC.

Acknowledgements

We gratefully acknowledge financial support from the 973 Program (2011CBA00505, 2013CB933200), the Strategic Priority Research Program of Chinese Academy of Sciences (XDA09030102), the NSF of China (21403237, 21303202, 21303203), and the NSF of Fujian Province (2014J05025).

Notes and references

[a] *State Key Laboratory of Structural Chemistry, Fujian Institute of Research on the Structure of Matter, Chinese Academy of Sciences, Fuzhou, Fujian 350002, P. R. China. E-mail: gcguo@fjirsm.ac.cn, znxu@fjirsm.ac.cn; Fax: +86-591-83714946; Tel: +86-591-83512502*

[b] *Key Laboratory of Coal to Ethylene Glycol and Its Related Technology, Chinese Academy of Sciences, Fuzhou, Fujian 350002, P. R. China*
† Electronic Supplementary Information (ESI) available: XRD patterns, BET surface area, XPS spectrum, *in situ* DRIR spectra, GC diagrams. See DOI: 10.1039/b000000x/

1. A.-A. G. Shaikh and S. Sivaram, *Chem. Rev.*, 1996, **96**, 951-976.
2. P. Tundo and M. Selva, *Acc. Chem. Res.*, 2002, **35**, 706-716.
3. S. T. King, *J. Catal.*, 1996, **161**, 530-538.
4. J.-Q. Wang, J. Sun, W.-G. Cheng, C.-Y. Shi, K. Dong, X.-P. Zhang and S.-J. Zhang, *Catal. Sci. Technol.*, 2012, **2**, 600-605.
5. M.-S. Park, G.-X. Wang, Y.-M. Kang, D. Wexler, S.-X. Dou and H.-K. Liu, *Angew. Chem. Int. Ed.*, 2007, **46**, 750-753.
6. H. Babad and A. G. Zeiler, *Chem. Rev.*, 1973, **73**, 75-91.
7. J. Xu, K.-Z. Long, T. Chen, B. Xue, Y.-X. Li and Y. Cao, *Catal. Sci. Technol.*, 2013, **3**, 3192-3199.
8. N. Keller, G. Rebmann and V. Keller, *J. Mol. Catal. A-Chem.*, 2010, **317**, 1-18.
9. H.-Y. Zheng, J. Ren, Y. Zhou, Y.-Y. Niu and Z. Li, *J. Fuel Chem. Technol.*, 2011, **39**, 282-286.
10. T. Sakakura and K. Kohno, *Chem. Commun.*, 2009, **11**, 1312-1330.
11. A. Bansode and A. Urakawa, *ACS Catal.*, 2014, **4**, 3877-3880.
12. M. J. Schneider, M. Haumann, M. Stricker, J. Sundermeyer and P. Wasserscheid, *J. Catal.*, 2014, **309**, 71-78.
13. Y. Yamamoto, T. Matsuzaki, S. Tanaka, K. Nishihira, K. Ohdan, A. Nakamura and Y. Okamoto, *J. Chem. Soc., Faraday T rans.*, 1997, **93**, 3721-3727.
14. Y. Dong, S. Huang, S. Wang, Y. Zhao, J. Gong and X. Ma, *ChemCatChem*, 2013, **5**, 2174-2177.
15. T. Matsuzaki and A. Nakamura, *Catal. Surv. Japan*, 1997, **1**, 77-88.
16. Z.-N. Xu, J. Sun, C.-S. Lin, X.-M. Jiang, Q.-S. Chen, S.-Y. Peng, M.-S. Wang and G.-C. Guo, *ACS Catal.*, 2013, **3**, 118-122.
17. S.-Y. Peng, Z.-N. Xu, Q.-S. Chen, Y.-M. Chen, J. Sun, Z.-Q. Wang, M.-S. Wang and G.-C. Guo, *Chem. Commun.*, 2013, **49**, 5718-5720.
18. S.-Y. Peng, Z.-N. Xu, Q.-S. Chen, Z.-Q. Wang, Y. Chen, D.-M. Lv, G. Lu and G.-C. Guo, *Catal. Sci. Technol.*, 2014, **4**, 1925-1930.
19. X. Zheng, H. Lin, J. Zheng, X. Duan and Y. Yuan, *ACS Catal.*, 2013, **3**, 2738-2749.
20. Y. Ge, Y. Dong, S. Wang, Y. Zhao, J. Lv and X. Ma, *Front. Chem. Sci. Eng.*, 2012, **6**, 415-422.
21. Y. Yamamoto, *Catal. Surv. Asia.*, 2010, **14**, 103-110.
22. D. Wang, F. Gao, C. H. F. Peden, J. Li, K. Kamasamudram and W. S. Epling, *ChemCatChem*, 2014, **6**, 1579-1583.
23. D. Wang, Y. Jangjou, Y. Liu, M. K. Sharma, J. Luo, J. Li, K. Kamasamudram and W. S. Epling, *Appl. Catal. B-Environ.*, 2015, **165**, 438-445.
24. S. Chen, Y. Meng, Y. Zhao, X. Ma and J. Gong, *AIChE Journal*, 2013, **59**, 2587-2593.
25. S. Chen, S. Wang, X. Ma and J. Gong, *Chem. Commun.*, 2011, **47**, 9345-9347.
26. Y. Meng, T. Wang, S. Chen, Y. Zhao, X. Ma and J. Gong, *Appl. Catal. B-Environ.*, 2014, **160-161**, 161-172.
27. R. Jiang, Y. Wang, X. Zhao, S. Wang, C. Jin and C. Zhang, *J. Mol. Catal. A-Chem.*, 2002, **185**, 159-166.
28. J. W. Choung, I.-S. Nam, *Appl. Catal. B-Environ.*, 2006, **64**, 42-50.
29. Y. Yuan, W. Cao, W. Weng , *J. Catal.*, 2004, **228**, 311-320.
30. T. Baidya, P. Bera, B. D. Mukri, S. K. Parida, O. Kröcher, M. Elsener and M. S. Hegdea, *J. Catal.*, 2013, **303**, 117-129.
31. M. Jabłonska, A. Król, E. Kukulska-Zajac, K. Tarach, L. Chmielarz and K. Góra-Marek, *J. Catal.*, 2014, **316**, 36-46.
32. O. Dulaurent, K. Chandes, C. Bouly and D. Bianchi, *J. Catal.*, 1999, **188**, 237-251.
33. H. Unterhalt, P. Galletto, M. Morkel, G. Rupprechter and H.-J. Freund, *Phys. Stat. Sol. (a)*, 2001, **188**, 1495-1503.
34. Y. Ji, G. Liu, W. Li and W. Xiao, *J. Mol. Catal. A-Chem.*, 2009, **314**, 63-70.
35. X.-G. Zhao, Q. Lin and W.-D. Xiao, *Appl. Catal. A-Gen.*, 2005, **284**, 253-257.
36. L. A. Pressley, E. D. Pylant and J. M. White, *Surf. Sci.*, 1996, **367**, 1-19.
37. Z.-Z. Wang, S.-Y. Huang, Y.-L. Shen, S.-P. Wang and X.-B. Ma, *J. Fuel Chem. Technol.*, 2012, **40**, 1212-1221.
38. Y. Zhang and A. T. Bell, *J. Catal.*, 2008, **255**, 153-161.
39. T. Beutel, *J. Chem. Soc., Faraday Trans.*, 1998, **94**, 985-993.